Research Article | Vol. 27, No. 17 | 19 Aug 2019 | OPTICS EXPRESS 23830
Optics EXPRESS

Optical polarization rogue waves from supercontinuum generation in zero dispersion fiber pumped by dissipative soliton

LEI GAO,[1,4] LINGDI KONG,[1] YULONG CAO,[1] STEFAN WABNITZ,[2,3] HONGQING RAN,[1] YUJIA LI,[1] WEI HUANG,[1] LIGANG HUANG,[1] MIN LIU,[1] AND TAO ZHU[1,5]

[1]*Key Laboratory of Optoelectronic Technology & Systems (Ministry of Education), Chongqing University, Chongqing 400044, China*
[2]*Dipartimento di Ingegneria dell'Informazione, Elettronica e Telecomunicazioni, Sapienza Università di Roma, Via Eudossiana 18, 00184 Rome, Italy*
[3]*Novosibirsk State University, 1 Pirogova str, Novosibirsk 630090, Russia*
[4]*gaolei@cqu.edu.cn*
[5]*zhutao@cqu.edu.cn*

Abstract: Optical rogue waves emerge in nonlinear optical systems with extremely large amplitudes, and leave without a trace. In this work, we reveal the emergence of optical polarization rogue waves in supercontinuum generation from a zero-dispersion fiber, pumped by a dissipative soliton laser. Flat spectral broadening is achieved by modulation instability, followed by cascaded four-wave-mixing. In this process, we identify the emergence of optical polarization rogue waves, based on the probability density function of the relative distance among polarization states. Experimental results show that optical polarization rogue waves originate from vector multi-wave-mixing. Besides, we observe double peaks, and even triple peaks in the histogram of the state of polarization. This is a new and intriguing property, never observed so far in optical rogue waves, for example those emerging in the statistics of pulse intensities. Our polarization domain statistical analysis provides a new insight into the still debated topic of the mechanism for rogue wave generation in optical supercontinuum.

1. Introduction

Rogue waves (RWs) are known as extremely large amplitude waves, which propagate in open oceans. They are rare events that emerge with unexpectedly large probabilities, deviating from the power law wave-amplitude statistics which are typical for random processes, and leave without a trace [1–3]. RWs can be experimentally identified by the presence of heavy-tailed statistics, typically L-shaped, describing the appearance of rare events. Different RWS mechanisms have been proposed so far: from the simple linear random superposition of independent weak waves, to nonlinear effects such as modulation instability (MI) and the subsequent formation of localized breathers. When the coherence of a physical system is deteriorated, RWs with diverse parameters may occur in different dimensions [2]. Additional examples include: the fluence profiles of multi-filaments, liquid helium, and high intensity pulses in supercontinuum generation (SCG) in optical fibers [4–17].

Due to phenomenological and physical analogies between extreme events in optics and hydrodynamics, D. R. Solli et al. introduced the concept of optical RWs, associated with a long-tailed intensity histogram in the long-wavelength range of fiber optical supercontinuum spectra [5]. Much research has been dedicated to finding RW solutions of the nonlinear Schrödinger equation in different physical systems: various kinds of breathers have been proposed as examples of optical RWs [6]. Recently, real-time detection techniques, such as the dispersive Fourier transform and time-lens, have been utilized to identify the presence of coherent pulses with extremely high intensities. An abrupt phase change across the pulse

#368071 https://doi.org/10.1364/OE.27.023830
Journal © 2019 Received 21 May 2019; revised 12 Jul 2019; accepted 18 Jul 2019; published 5 Aug 2019

Optics EXPRESS

profile was found to be associated with optical RWs [12,13]. The presence of a RWs is identified by a trough-to-crest height larger than 2 times the significant wave height (SWH). Moreover, the occurrence of RWs in optics can be identified in different domains: for example, in the pulse intensity for the time domain [5], in the spectral width for the frequency domain [14], in the spatial intensity in a two-dimensional camera image [15], the depth of dark pulses [18], and the presence of spectrally narrowband pulses with a right-skewed distribution [19]. For a full investigation of the emergence optical RWs, additional dimensions can be introduced.

Similar to optical RWs in the temporal or spectral domains, the emergence of irregular behavior in the state of polarization (SOP) may also be investigated. We propose to investigate the emergence of optical polarization rogue waves (PRWs), which can be identified by measuring the relative distance, r, between any two points on the Poincaré sphere

$$r = \left|S_m - S_n\right| = 2\sin^{-1}(\sqrt{(S_{m1} - S_{n1})^2 + (S_{m2} - S_{n2})^2 + (S_{m3} - S_{n3})^2}\,/\,2) \qquad (1)$$

where $S = (s_1, s_2, s_3)$ is the Stokes vector representation of the SOP for a specific wavelength [11]. In order to characterize PRWs during supercontinuum generation from a noise seed, we perform N independent detections of the SOP for a specific wavelength, at particular pump power. As long as N is large enough, the detected polarization distribution is accurate enough to characterize the SOP of this wavelength. The number of N can be evaluated during the experimental detection. By counting the probability of r, one obtains a distribution histogram, which can be used for identifying the presence of optical PRWs. The interpretation of PRWs is different from the case of RWs in temporal or spectral domains: the latter denote the generation of giant pulses with high amplitude or bandwidth, whereas PRWs describe the emergence of particular wavelengths, whose SOP distribution largely deviates from a purely random (i.e., Gaussian) distribution. As a matter of fact, rogue polarization states appear more frequently than expected from a Gaussian distribution. Their appearance is accompanied with a deteriorated coherence in the nonlinear system, such as during supercontinuum generation, or even optical turbulence.

Here, we investigate the polarization dynamics of SCG in a zero-dispersion fiber (ZDF), pumped by a dissipative soliton (DS) laser. First, we observe spectral broadening through MI, and subsequently cascaded four-wave-mixing (FWM). By filtering the optical wavelengths at different stages of the SCG, we find that frequencies generated by primary MI are scalar. Their polarizations are well defined. Fluctuations occur only around the edge of the spectrum. The scalar frequencies are different from those generated by vector FWM process, in which frequencies tend to be scattering. In the SCG process, we identify the existence of optical PRWs based on the SWH method.

2. Experimental setup

Figure 1(a) schematically depicts the experimental setup, consisting of a DS laser source, compressed and amplified by a commercial high gain erbium-doped fiber amplifier (AEDFA-23-B-FA, Amonic), and injected into 20 m of highly nonlinear fiber with zero dispersion at 1550 nm. The commercially available ZDF has an effective diameter of 3.86 μm and a nonlinear coefficient of 10 $W^{-1}km^{-1}$. The dispersion slope is less than 0.02 $ps/nm^2/km$. Such a fiber facilitates phase matching of FWM over an ultra-broad frequency range, and octave-spanning spectrum can be easily obtained. In our experiment, primary sidebands are generated by MI. Next, new frequencies are generated by cascaded FWM among those sidebands and the DS spectrum. Namely, all FWM procedures are possible. Primarily, we observe the MI with a degenerate FWM process. When the power of the DS is relatively small, new frequencies are generated in a forward direction, namely, energy flows from the DS spectrum into the sidebands. However, when the DS power is large enough, the direction

Optics EXPRESS

of energy flow may also occur in a backward direction, namely, from the FWM components back into the DS spectrum. During SCG, a transition from high to low spectral coherence may be controlled by varying the pump pulse peak power. Consequently, RWs in temporal, spectral, and polarization domains emerge in the SCG process. Here, we limit our attention to optical PRWs. After SCG, light at the fiber output is filtered by a tunable thin-film optical filter (TF, Santec, OTF-320) with a bandwidth of 0.2 nm. The output SOP is detected by a high-speed polarization state analyzer (PSA).

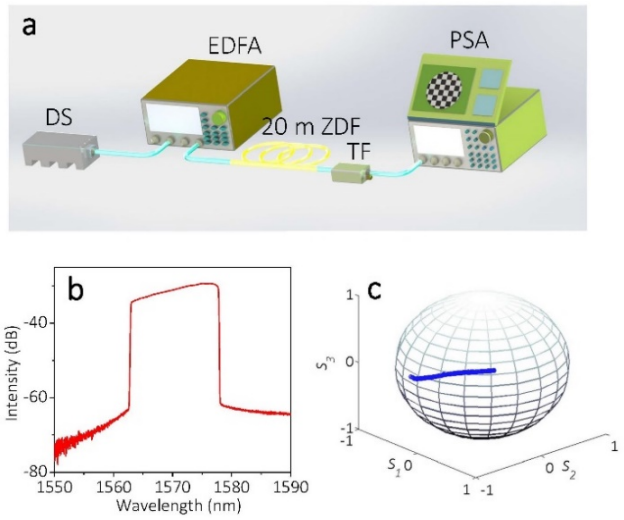

Fig. 1. (a) Schematic of the experimental setup and measurement. (b) Optical spectrum of the DS. (c) SOPs of DS after a tunable thin-film filter.

The average power from the home-made DS laser is 0.5 mW. Figure 1(b) depicts its rectangle-shaped optical spectrum ranging from 1562.9 nm to 1577.9 nm, with a full width at half maximum of 15 nm. The DS pulse duration is 29 ps. After the EDFA, the average power is amplified up to 100 mW, and the pulse duration is compressed down to 1.5 ps. In Fig. 1(c), we illustrate the SOP distribution across all filtered wavelengths of the SC. The linear distribution of points on the Poincaré sphere originates from the wavelength-dependent SOP rotation imposed by the TF. In fact, the SOP of the DS, especially in its central spectral region, remains a constant with wavelength. The amplification process in EDFA does not change the SOP distribution, hence the amplified optical spectrum is expected to exhibit a constant SOP.

3. Results and discussion

Figure 2(a) shows the SCG optical spectrum for various pump powers. The pump power increases with a step of 1mW. As our data are limited by the measurement range of the optical spectrum analyzer (Yokogawa, AQ6370), we only give data in the range between 1000 nm and 1700 nm. The SC is rather flat for a pump power of 100 mW after the EDFA: the 3 dB flatness in the blue side can be larger than 350 nm. According to the characteristics of the formed spectrum for different pump powers, we classified the SCG process into two different stages: (1) the scalar stage, (2) the vector stage. The corresponding spectra are superimposed in Fig. 2(b). For a pump power of 15 mW, we observe a scalar stage, where cascaded symmetric sidebands are generated around the DS spectrum.

Different orders of Stokes and anti-Stokes sidebands appear. The gain g(Ω) of the primary MI sidebands reads as

Optics EXPRESS

$$g(\Omega) = |\beta_2 W| \sqrt{\left(\frac{4\gamma P}{|\beta_2|} - \Omega^2\right)} \tag{2}$$

where β_2, γ, and P are the group velocity dispersion (GVD), the nonlinear coefficient, and the peak power, respectively [20]. For example, the frequency shift of the first Stokes and anti-Stokes sidebands is 4.62 THz for pump power at 15 mW. Owing to the nominally zero GVD, the observed sideband shifts are unusually large, and they increase with the power of the amplified DS.

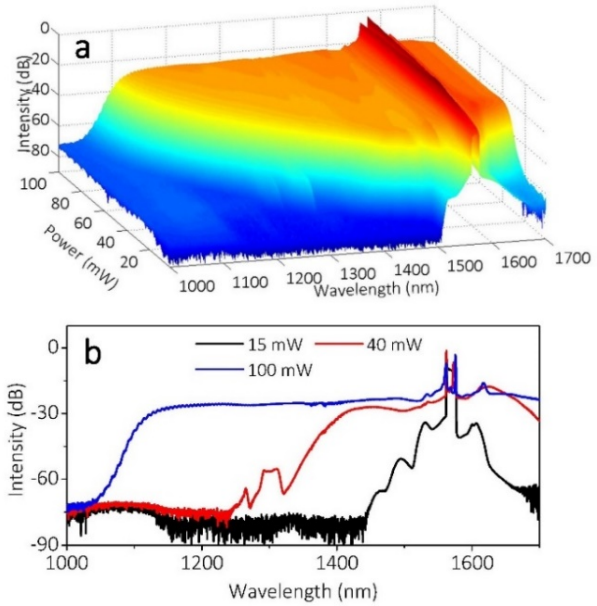

Fig. 2. (a) SCG for different pump powers of the amplified DS. (b) Superimposed optical spectra from (a) for a pump power of 15 mW, 40 mW, and 100 mW, respectively.

After the scalar stage, a slight interference pattern appears on the spectrum, indicating that new frequencies are generated by different processes. For a pump power of 40 mW, vector FWMs contributes to spectrum broadening. Here, new frequencies are generated within both forward and backward directions (that is, in and out of the DS pump spectrum). Finally, a broad and flat spectrum is formed via the merging of all FWMs processes.

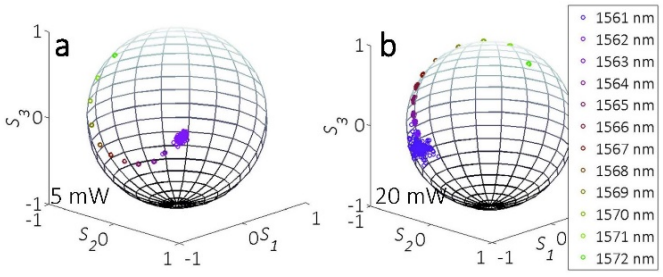

Fig. 3. (a)-(b) SOPs of SC in the range between1562 nm and 1572 nm, for a pump power of 5 mW and 20 mW, respectively. Wavelengths in (a) are represented by the same colors in (b).

The transition from the scalar to the vector stage of SCG is accompanied by a coherence deterioration, a property which is more evident when studied in the polarization domain. To detect the SOP of each wavelength as precisely as possible, the filter resolution should be

Optics EXPRESS

small enough. The resolution and tuning range of the filter that we used are 0.2 nm and 1530 to 1610 nm, respectively. Besides, there is a discontinuity at 1572 nm. Therefore, we only give experimental data in the range of 1562 nm to 1572 nm in Figs. 3(a) and 3(b). They depict the SOPs of different frequencies for pump powers of 5 mW and 20 mW, respectively. We obtain 5000 SOPs for each case. It is clear that the SOPs in the scalar stage are well defined, i.e., they lie within a small spot on the Poinceré sphere. Fluctuations only occur around the edge of the spectrum (i.e., around 1562 nm).

On the other hand, SOPs tends to be scattered around in the vector stage, as shown in Figs. 4(a)-4(f). Similarly, 5000 points are exhibited for each case. For pump powers larger than 30 mW, for each selected wavelength the SOPs corresponding to different realization of the SC scatter in a broad area, with a center that is continuously tuned by pump power. Meanwhile, the degree of dispersion of SOP scattering increases with DS pump power. The reason is clear: stronger FWMs cascades in those frequencies, where the corresponding phase-matching conditions can be easily satisfied, owing to the nearly-zero dispersion in this range. The larger the pump power of the DS source, the stronger the cascaded FWM process. Eventually, the phases of newly generated frequencies are loosely fixed and become chaotic, leading to optical turbulence. This process deteriorates the coherence of the SCG process. For wavelengths generated in the stage where there is a loss of coherence, SOPs are randomly scattered on the Poincaré sphere. Phase-matching conditions are stochastic for wavelengths located far away from the center of the DS spectrum. Therefore, it is natural to anticipate the possible generation of RWs in intensity, spectrum, or polarization for wavelengths belonging to blue-shifted or red-shifted portions of the SC.

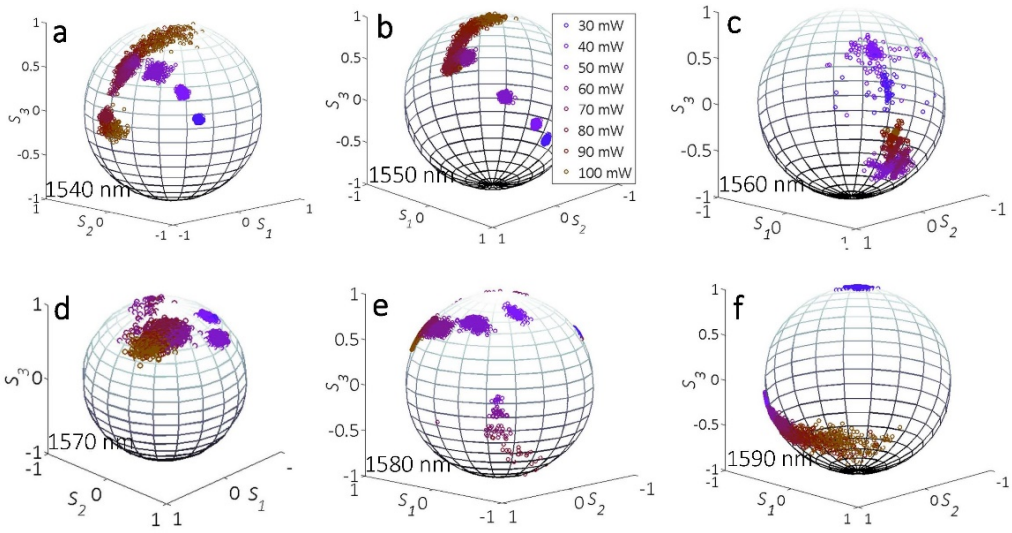

Fig. 4. (a)-(f) SOPs for various wavelengths and pump powers from 30 mW to 100 mW. Pump powers in (a), and (c)-(f) are represented by the same colors as in (b). Specifically, cross-shaped lines of SOPs in (c) indicate the presence of vector FWM [9].

Primarily, we calculated the probability density function of SOPs obtained in different realizations of the SCG, based on the previously introduced relative distance *r*. The probabilities for different relative distances are calculated based on 5000 detections using Eq. (1). In fact, we find that the probabilities for detection larger than 2000 is accurate enough to reveal the distributing characteristics. Figure 5 shows the histograms at 1570 nm for different pump power values. This particular wavelength is representative of the behavior observed within the spectral range of the input DS. For a pump power of 40 mW, the probability distribution function of *r* is quasi-Gaussian (Fig. 5(a)).

Optics EXPRESS

Whereas, as depicted in Fig. 5(b), when the pump power grows above 70 mW the *r* distribution deviates from a Gaussian shape, and a heavy tail appears, corresponding to rogue SOPs (corresponding to large *r* values) . The histogram resembles a left-skewed probability function, similar to the case of temporal RWs [5]. Based on the SWH, which is defined as the mean amplitude of the largest third of the *r*, we identify the occurrence of optical PRWs whenever *r* is larger than twice of the SWH. Besides, the relative distance *r* is this case is ranging from 0 between 0.9, which is much larger than that for pump power 40 mW (0~0.2). The reason is that the SOPs tend to be more scattered. However, the probability to find PRWs for pump powers as high as 100 mW decreases unexpectedly, and the histogram returns to a Gaussian shape. The possible reason could be that frequencies within the DS spectrum undergo intense cascaded FWM in both forward and backward directions, so that the energy coupling among different wavelengths and SOPs is rapidly varying. New frequencies with larger *r* are generated, while they are also annihilated. All of these nonlinear processes take place in a probabilistic manner for subsequent SCG events. The corresponding statistics is determined by the pump power, and the phase-matching conditions.

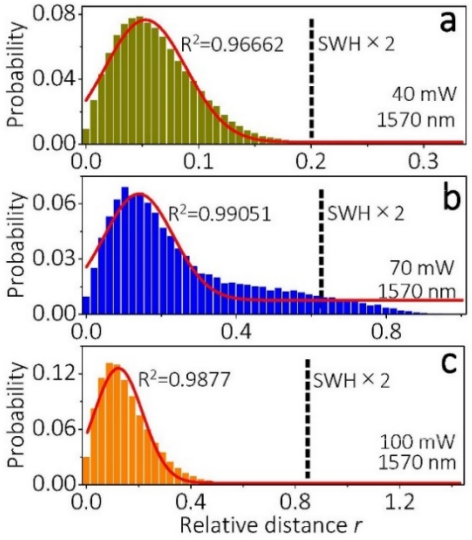

Fig. 5. Histograms for the filtered SC wavelength of 1570 nm, where the pump power is 40 mW (a), 70 mW (b), and 100 mW (c), respectively. They are fitted by Gaussian function.

In contrast, Figs. 6(a)-6(c) report the probability density functions of the relative distance *r* for wavelength at 1540 nm, which is representative of the behavior observed beyond the spectral range of the input DS: similar results were found in the red-shifted side in the SC as well. It is clear that more rogue SOPs are detected when pump power is equal to 70 mW, when comparing with the histogram for 40 mW of pump power. As shown in Fig. 6(c), the probability of observing *r* larger than 2* SWH is much larger for a pump power as high as 100 mW. The probability of a high relative distance *r* around 0.6 is increased, at the expense of strong depletion of *r* values less than 0.1. This is associated with the presence of a much stronger heavy tail in the histogram, associated with PRWs. However, we notice that the distribution of the relative distances *r* in Fig. 6(c) exhibits two distinct probability density distributions (PDFs)). The second PDF is well fitted by a Gaussian shape. This puts into question whether RWs obey their own random wave statistics, which takes the form of a heavy tail. The reason for the emergence of the secondary Gaussian PDF can be inferred from Fig. 4(a). Here it can be seen that a secondary population of SOPs is formed for pump powers larger than 80 mW. The underlying physics is clear: the coexisting PDFs of SOP originate from the vector stage of SCG. These experimental results indicate that the PDF of PRWs

Optics EXPRESS

depends on the specific SCG process. For relative weak pump powers and in the scalar stage, the key parameter is the intensity of the cascaded FMW, which is controlled via the power of the DS pump. Whereas for stronger pump powers, the vector stage of SCG leads to multiple PDFs of SOP. The corresponding identification of PRWs requires further investigations.

Similarly, Figs. 6 (d)-6(f) report the PDFs of r for wavelength at 1580 nm, which is located in the red-shifted side of the SC. For a pump power of 40 mW, the histogram deviates from a Gaussian shape, and the probability of PRWs remains low. We observe a second PDF when the pump power reaches 70 mW, which subsequently vanishes for pump powers of 100 mW. During the SCG process, for some wavelengths rare PRWs probabilities are detected, as shown in Figs. 3(e), 6 (e) and 6(f). The analysis of the corresponding PDFs in the region with r >2 gives a measure of the probability of observing PRWs in SCG.

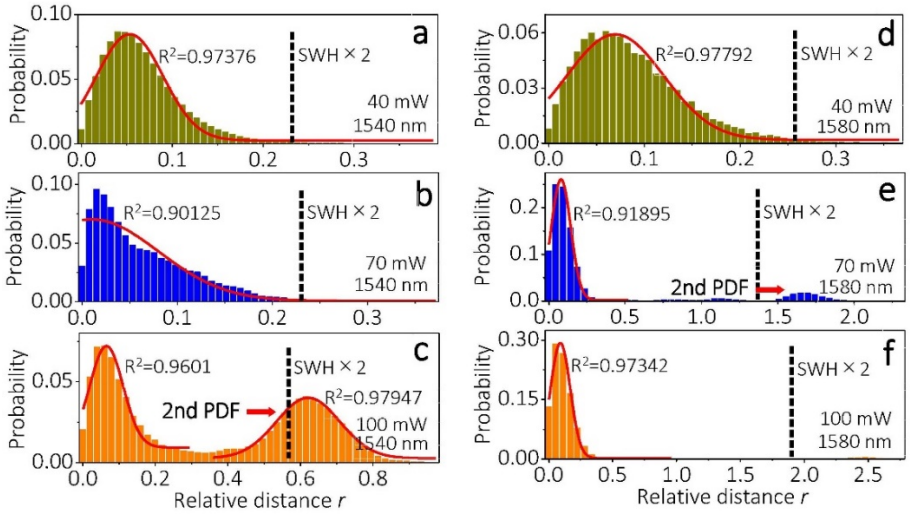

Fig. 6. Histograms for the filtered SC wavelength of 1540 nm ((a)-(c)) and 1580 nm ((d)-(f)), where the pump power is 40 mW, 70 mW, and 100 mW, respectively.

To further characterize the emergence of PRWs in SCG, we calculate the PDFs of SOP for wavelengths ranging from 1541 nm to 1557 nm. Figure 7(a) illustrates their SOPs values, for a fixed pump power of 100 mW. As can be seen, SOPs emerging at 1557 nm are scattered within a single domain. Whereas, as the wavelength is blue-shifted, the SOPs evolve into two separate domains. For wavelengths situated even farther away from the DS pump (e.g., for wavelengths smaller than 1549 nm), the corresponding SOPs scatter within three different domains, which are continuously interchanging their energy. Those wavelengths are generated by vector FWM processes, which occur among all possible polarization interactions in a nonpolarization maintaining fiber. The emergence of multiple SOP domains on the Poincaré sphere originates from the coexistence of these multiple processes of cascaded, and phase-matched FWM processes, exchanging energy with the pump in both forward and backward directions along the frequency axis.

For wavelengths between 1543 nm and 1547 nm, the corresponding histograms in Figs. 7(b)-7(f) clearly denote the existence of optical PRWs. For 100 mW pumped SC, the histograms are highly sensitive to the specific filtered wavelength. For example, at 1543 nm and 1547 nm, SOPs with rogue positions are observed on the Poincaré sphere, as denoted by the heavy tails at large r values. However, double PDFs, and even triple PDFs may appear, depending on the wavelength that we selected. Again, for strong pumping conditions, multiple phase-matching conditions can be satisfied, and the proportion of cascaded FWMs within forward and backward directions are constantly varying along the fiber. As a result, energy continuously flows among different wavelengths.

Optics EXPRESS

Compare with the intensity distributions for conventional RWs [5–8], the PRWs in SCG are slightly different. Quantitatively, PRWs are identified based on the PDF of relative distance, *r*, between any two points on the Poincaré sphere for the single frequency, while conventional RWs denote the emergence of ultrahigh intensities within a wide frequencies. The corresponding temporal intensities for PRWs may not be large enough, even may be ultrasmall when we consider the forming procedure. The PRWs are more than the polarization aspect of the conventional RWs. However, we also believe that there is a connection between the PRWs and conventional RWs, as they are both formed only under high nonlinear process. A more convincing and reliable investigation between them requires single-shot measurement of the intensity and polarizations simultaneously, together with more rigorous theoretical analysis.

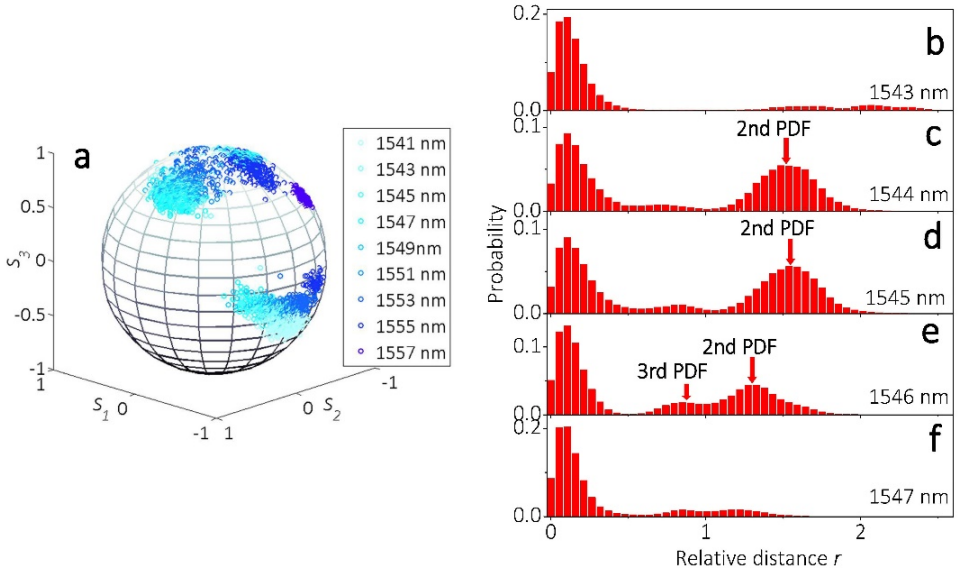

Fig. 7. (a) SOPs for wavelengths between 1541 nm and 1557 nm at the pump power of 100 mW. (b)-(f) Histograms for wavelengths between 1543 nm and 1547 nm for pump power at 100 mW.

When considering the above experimental results and discussions, two main issue emerge in the process of SCG in zero dispersion fiber. The first issue is that given the complex polarization evolutions, whenever the zero-dispersion limit is approached, simple models based on integrable scalar or vector nonlinear Schrödinger equations should be extended, by including contributions from all possible vector interactions leading to FWM-induced energy exchanges among polarizations. This is of particular importance for large pump powers, where the phase-matching conditions are satisfied easily, and nonlinear processes take place probabilistically. The second issue is that the study of RWs in SCG, as well as any coherence-deteriorated physical system, requires a more rigorous reexamination. For example, it is not clear if the presence of multiple PDFs in the histograms for the SOPs should be associated with the presence of PRWs, although a heavy tail is shown. In fact, when we only consider pulse intensities at any filtered wavelength in a nonlinear optical system, contributions from all SOPs are summed together. A broader and more complete picture of RW generation will require obtaining statistical data across different dimensions, i.e., temporal, spectral, and polarization domains.

4. Conclusion

In summary, we investigated the emergence of optical PRWs associated with SCG in a zero-dispersion fiber, pumped by DS laser pulses. Spectral broadening results first from scalar MI,

Optics EXPRESS

followed by cascaded vector FWM processes. In the vector stage, optical PRWs are identified on the basis of the significant wave height method. Our results unveil a new aspect of optical RW formation in supercontinuum generation, which provides a complementary aspect of RW generation in nonlinear optical systems. The observed complex polarization evolutions clearly point out that, whenever the zero-dispersion limit is approached, simple models based on integrable scalar or vector nonlinear Schrödinger equations should be extended, by including contributions from vector FWM processes leading to polarization energy exchanges.

Funding

Natural Science Foundation of China (61705023, 61635004, 61475029); National Postdoctoral Program for Innovative Talents (BX201600200); General Financial Grant from the China Postdoctoral Science Foundation (2017M610589); Science Foundation of Chongqing (CSTC2017JCYJA0651); Science and Technology on Plasma Physics Laboratory (6142A0403050817); Ministry of Education and Science of the Russian Federation (14.Y26.31.0017).

References

1. C. Kharif and E. Pelinovsky, "Physical mechanisms of the rogue wave phenomenon," Eur. J. Mech. BFluids **22**(6), 603–634 (2003).
2. M. Onorato, S. Residori, U. Bortolozzo, A. Montina, and F. T. Arecchi, "Rogue waves and their generating mechanisms in different physical contexts," Phys. Rep. **528**(2), 47–89 (2013).
3. J.-P. Eckmann, "Roads to turbulence in dissipative dynamical systems," Rev. Mod. Phys. **53**(4), 643–654 (1981).
4. S. Birkholz, E. T. J. Nibbering, C. Brée, S. Skupin, A. Demircan, G. Genty, and G. Steinmeyer, "Spatiotemporal rogue events in optical multiple filamentation," Phys. Rev. Lett. **111**(24), 243903 (2013).
5. D. R. Solli, C. Ropers, P. Koonath, and B. Jalali, "Optical rogue waves," Nature **450**(7172), 1054–1057 (2007).
6. J. M. Dudley, F. Dias, M. Erkintalo, and G. Genty, "Instabilities, breathers and rogue waves in optics," Nat. Photonics **8**(10), 755–764 (2014).
7. C. Lecaplain, P. Grelu, J. M. Soto-Crespo, and N. Akhmediev, "Dissipative rogue waves generated by chaotic pulse bunching in a mode-locked laser," Phys. Rev. Lett. **108**(23), 233901 (2012).
8. Z. Liu, S. Zhang, and F. W. Wise, "Rogue waves in a normal-dispersion fiber laser," Opt. Lett. **40**(7), 1366–1369 (2015).
9. L. Gao, T. Zhu, S. Wabnitz, M. Liu, and W. Huang, "Coherence loss of partially mode-locked fibre laser," Sci. Rep. **6**(1), 24995 (2016).
10. D. V. Churkin, S. Sugavanam, N. Tarasov, S. Khorev, S. V. Smirnov, S. M. Kobtsev, and S. K. Turitsyn, "Stochasticity, periodicity and localized light structures in partially mode-locked fibre lasers," Nat. Commun. **6**(1), 7004 (2015).
11. L. Gao, T. Zhu, S. Wabnitz, Y. Li, X. S. Tang, and Y. L. Cao, "Optical puff mediated laminar-turbulent polarization transition," Opt. Express **26**(5), 6103–6113 (2018).
12. P. Suret, R. E. Koussaifi, A. Tikan, C. Evain, S. Randoux, C. Szwaj, and S. Bielawski, "Single-shot observation of optical rogue waves in integrable turbulence using time microscopy," Nat. Commun. **7**(1), 13136 (2016).
13. M. Närhi, B. Wetzel, C. Billet, S. Toenger, T. Sylvestre, J. M. Merolla, R. Morandotti, F. Dias, G. Genty, and J. M. Dudley, "Real-time measurements of spontaneous breathers and rogue wave events in optical fibre modulation instability," Nat. Commun. **7**(1), 13675 (2016).
14. J. M. Dudley, G. Genty, and B. J. Eggleton, "Harnessing and control of optical rogue waves in supercontinuum generation," Opt. Express **16**(6), 3644–3651 (2008).
15. R. Höhmann, U. Kuhl, H. J. Stöckmann, L. Kaplan, and E. J. Heller, "Freak waves in the linear regime: a microwave study," Phys. Rev. Lett. **104**(9), 093901 (2010).
16. S. A. Kolpakov, H. Kbashi, and S. V. Sergeyev, "Dynamics of vector rogue waves in a fiber laser with a ring cavity," Optica **3**(8), 870–875 (2016).
17. K. Krupa, K. Nithyanandan, and P. Grelu, "Vector dynamics of incoherent dissipative optical solitons," Optica **4**(10), 1239–1244 (2017).
18. B. Frisquet, B. Kibler, P. Morin, F. Baronio, M. Conforti, G. Millot, and S. Wabnitz, "Optical dark rogue wave," Sci. Rep. **6**(1), 20785 (2016).
19. D. R. Solli, C. Ropers, and B. Jalali, "Rare frustration of optical supercontinuum generation," Appl. Phys. Lett. **96**(15), 151108 (2010).
20. K. Tai, A. Hasegawa, and A. Tomita, "Observation of modulational instability in optical fibers," Phys. Rev. Lett. **56**(2), 135–138 (1986).